Tellus (1985), *37A*, 336–360

On the structure of the 30 to 50 day mode over the globe during FGGE

By T. N. KRISHNAMURTI and SULOCHANA GADGIL, *Department of Meteorology, Florida State University, Tallahassee, FL 32306, USA*

(Manuscript received May 4, 1984; in final form January 31, 1985)

ABSTRACT

6 vertical levels of the entire 365-day global FGGE IIIb analysis for 5 variables are subjected to a time-series analysis and a frequency filter to investigate the structure of the 30- to 50-day mode. This study isolates regions where the amplitude of these low-frequency oscillations are large; the vertical structures across these large amplitude regions are also presented. The seasonal variation of the maximum 30–50 day filtered wind in the lower troposphere is highlighted. The major results for the FGGE year show that the 30- to 50-day mode has its largest amplitude in the upper troposphere of polar latitudes and in the summer monsoon region. During the northern winter, active regions are also located over the equatorial belt of the central Pacific ocean. The phase propagation on the pressure surfaces are examined simply from an analysis of a time sequence of low-frequency weather maps. The vertical phase propagation is illustrated by pressure-time plots of the low-frequency data sets at individual locations. This analysis suggests vertical propagation over convective areas and a lack of it over most other regions.

A highlight of this study is a phenomenon we have labelled as "low-frequency storms". Here we illustrate long-lasting, low-frequency, weather systems that propagate meridionally (1) over the summer monsoon regions from the equator to the Himalayas and (2) over the eastern Pacific ocean from the equator northwards during the northern winter season. An example of such a long-lasting system is traced to 60° N; subsequently, it appears to move zonally from the gulf of Alaska across the Canadian Arctic, north Atlantic, and Europe prior to its dissipation over Siberia. The potential for interactions between these low-frequency systems and polar front cyclones is another interesting aspect of this investigation. The low-frequency oscillations and motions are considered important since their amplitude in the troposphere is large (8 ms^{-1}) and they are well-defined within their scales of motion (on the order of 4000 km or larger).

1. Introduction

Considerable interest has been evoked concerning the 40- to 50-day oscillations in the last decade. Madden and Julian's (1971, 1972) work dealing with the near equatorial sea-level pressure field and zonal wind clearly demonstrated a dominant oscillation in this time frame, apparently oriented primarily in the zonal plane. Yasunari (1980, 1981) examined the fluctuations in cloud cover over the Indian monsoon region and noted a meridional propagation of cloudiness anomalies in the period range of around 40 days. Using data sets for the summer season for 1969, Yasunari also confirmed the existence of zonal wind oscillations on this time frame. A detailed analysis of cloud cover over the summer monsoon region was presented by Sikka and Gadgil (1980), where fluctuations in cloud activity on this time scale were related to active and inactive spells of the Asian monsoon. They noted zonally-oriented cloud bands that move northwards from near-equatorial latitudes throughout the summer season. This result was also evident in the spectral analysis and frequency filtered fields of Yasunari.

From these studies, the authors were left with the impression that there was an equatorially-trapped pressure oscillation on the zonal plane as described

by Madden and Julian. In addition, Krishnamurti and Subrahmanyam (1982) noted from the data sets provided by the Monsoon experiment that there were meridionally-propagating, low-frequency, weather systems, especially over the Asian monsoon region. They also found that there was indeed a strong power in the period range of 30 to 50 days, especially for the zonal winds. Frequency-filtered charts over the summer monsoon region revealed a steady meridional progression of troughs and ridges whose passage over central India coincided with active and inactive spells of weather. The present study is an extension of this observational work covering the entire globe, for the entire troposphere, including five variables and extending over the entire 365 days of the global experiment.

There has also been considerable theoretical interest on the mechanisms for the generation of these low-frequency oscillations (Anderson and Rosen, 1983; Chang, 1977; Stevens, 1983; Webster, 1983). Anderson and Rosen examined the structure and meridional propagation of zonally-oriented bands in the atmospheric angular momentum fields. Stevens attributes the importance of zonally-symmetric and asymmetric instabilities in the tropics as a means for exciting these low-frequency oscillations. He suggested that deep tropical convection can provide energy for the maintenance of these instabilities. The observations presented in this study appear to confirm a tropical energy source for these instabilities. Webster's study is largely based on results from a zonally-symmetric atmospheric general circulation model. He suggests that the meridional motion of the low-frequency mode is a consequence of the stabilization of the lower tropospheric air in the rain areas, while the region to their immediate north becomes more unstable and favors convective activity, thus generating meridional motion. The importance of surface forcing (e.g., ground wetness and the surface heat balance) is stressed as being an important component of this general circulation model. Krishnamurti and Bhalme (1976) also stressed the importance of surface heating and stability during active and inactive spells of the monsoon. The notion that inertial instability of the zonal flows for symmetric and asymmetric disturbances exist along the equator was addressed by the analysis of Dunkerton (1983) in this context. Four recent studies deal with the use of the FGGE data sets towards studies on the 30- to 50-day perturbations. Lorenc (1984) carried out an Empirical Orthogonal Function analysis of the 200 mb velocity potential field and confirmed the presence of a planetary scale eastward propagating divergence wave on this time scale. This 30- to 50-day wave was mapped in detail by Krishnamurti et al. (1985) who noted a strong relationship between the passage of the divergence wave with respect to the wet and dry spells over the monsoon region. T. Murakami et al. (1983) examined the contributions to the energy release (i.e., the omega-T correlation) for waves on this time scale over the monsoon region and noted that the wave was thermally direct. M. Murakami (1984) examined the satellite derived IR brightness, zonal flows and monsoon activity and confirmed a strong relationship on this time scale. Thus, it appears worthwhile to examine the observational aspects of these low-frequency motions globally. (A list of acronyms is presented in Table 1.)

Table 1. *Acronyms*

ECMWF	European Centre for Medium Range Weather Forecasting
FGGE	First GARP global experiment
IR	Infrared satellite observations of outgoing longwave radiation
ITCZ	Inter-tropical convergence zone
MONEX	Monsoon experiment
NCAR	National Center for Atmospheric Research
IIIb	Final grid point analyzed data for FGGE

2. Scope of present study

The present study is aimed at clarifying some observational aspects of low-frequency motions in the 30- to 50-day period range. Aside from the usual power-spectral analysis and delineation of regions of maximum activity, this study addresses the vertical structure across these regions. The 365 days of frequency-filtered data is examined in a seasonal context and regions of activity for the different seasons are mapped. Following M. Murakami (1979, 1983), Krishnamurti and Subrahmanyam (1982), we shall illustrate frequency-filtered charts of the motion field. Hovmöller type diagrams of the zonal wind on this time scale are

presented on a pressure-time representation to examine qualitatively the vertical propagation of phase.

3. Data sets

The analysis scheme of the ECMWF is based on Lorenc (1980). This is a 3-dimensional, multivariate, optimal interpolation scheme. This analysis scheme requires a first-guess field which is obtained from a 6-h prediction during which a 15-level global primitive model is employed with full physics; the data sets from a variety of platforms of the global experiment are assimilated in this phase of the initialization process. A complete description of the analysis scheme is described in Bengtsson et al. (1982). The analysis of the ECMWF is carried out at 10, 20, 30, 50, 70, 100, 150, 200, 250, 300, 400, 500, 700, 850 and 1000 mb on a latitude/longitude grid with a separation of 1·875°. The variables that are analyzed include the two horizontal wind components, temperature, relative humidity and sea level pressure.

After carrying out a limited-area, high (spatial) resolution, analysis of the low-frequency events in the 30- to 50-day period range we noted that the horizontal scale of the phenomena of interest are adequately described by a 10° latitude by 10° longitude mesh. In order to limit the computer storage problem on the space/time mix of data sets the authors decided to use such a lower horizontal resolution data subset from the ECMWF analysis. It should be noted that no smoothing is applied spatially to the ECMWF analysis; their gridded data are merely extracted on a lower resolution global grid. The present study utilizes every 6th grid point of the ECMWF over the entire globe. Fig. 1 illustrates the resultant of FGGE IIIb grid points (employed by the European Centre for Medium Range Weather Forecast (ECMWF) in their daily analyses) studied by the authors. Because our interest is limited here to the low-frequency motions, we have limited our study to one set of fields per day (at 12 GMT).

4. Power spectral analysis and geographical distribution

The 365 days of FGGE IIIb wind data sets were subjected to a standard power-spectral analysis at all of the individual grid points in Fig. 1. A time series q_k of once-daily data for the entire FGGE year is represented by

$$Q_k = \sum_{j=0}^{2N-1} q_k \, e^{i2jk/2n}, \qquad (1)$$

where $2N$ denotes the total number of data points and N denotes the number of coefficients. The coefficients Q_k are determined by a standard fast Fourier transform method following Endlich et al. (1969).

The power-spectral estimates are given by

$$G_k = \frac{2\Delta t}{2N} |Q_k|^2 \qquad k = 0, 1, 2, \ldots N-1, \qquad (2)$$

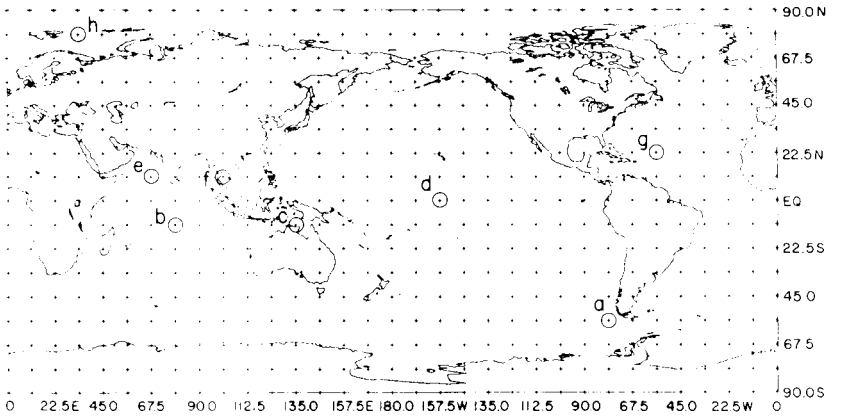

Fig. 1. The subset of FGGE IIIb grid points used in the present study.

where Δt is the time interval. Smoothed estimated may be obtained from the raw estimates of G_K by averaging L contiguous raw estimates to yield

$$G_{tK} = \sum_{j=-L/2}^{L/2} G_k(K+j)/L \tag{3}$$

The averaged power spectral estimates will be used to determine the response in various frequency bands of interest and will be illustrated following Zangvil (1977), where the product of the spectral estimates and the frequency is plotted as a function of the log of the frequency. The area under this curve retains the total variance of the spectrum. % variances R in various spectral windows with a frequency band-width $\Delta\nu$ are obtained by the simple normalization procedure

$$R = \left\{ \sum_{\nu=\nu_1}^{\nu_2} G_{tK} \sum_{\nu_L}^{\nu_U} G_{tK}\, \Delta\nu \right\} \times 100, \tag{4}$$

where $\Delta\nu = \nu_2 - \nu_1$ is a frequency interval and ν_L and ν_U denote the lower and upper limits of the frequency range covered in this study.

The statistical significance of 30 to 50 oscillations in global data sets for the FGGE year have been addressed by T. Murakami et al. (1983), Lorenc (1984) and by M. Murakami (1984). Since the pioneering work of Madden and Julian several investigators have examined the oscillations on this time scale. In our study we note that the zonal wind oscillations on this time scale have a rather large amplitude of the order of 3 to 8 m s^{-1}, e.g. Krishnamurti and Subrahmanyam (1982). Thus the statistical significance of the 30- to 50-day oscillation within the year long global data seem to be quite well established. The geographical distribution of the amplitude of this oscillation does exhibit considerable variability from region to region. This is of considerable interest in the present study.

We will next briefly discuss the frequency filter which is central to the objective of this study. The results of spectral analysis are summarized in this section as well.

4.1. *The frequency filter*

Following Murakami (1979) and Krishnamurti and Subrahmanyam (1982), a recursive filter was used to extract the filtered data sets into a 30- to 50-day time frame. The usual band-pass filters applied to a time series X_K produce a filtered series Y_K when X_K is multiplied by a series of weights W_l via a relationship of the type

$$Y_K = \sum_{l=-M}^{M} W_l X_{K+l}. \tag{5}$$

In general, since the band pass series Y_K depends on $2M$ weights, the so-called "end problem" arises (i.e., the filtered output series is shorter). The recursive filter, following Guillemin (1957) and Murakami (1979), is a function of the form

$$Y_K = a(X_K - X_{K-2}) - b_1 Y_{K-1} - b_2 Y_{K-2}. \tag{6}$$

Here a, b_1 and b_2 are weights given by the relations

$$a = \frac{2\Delta\Omega}{4 + 2\Delta\Omega + \Omega_0^2}, \tag{7}$$

$$b_1 = \frac{2(\Omega_0^2 - 4)}{4 + 2\Delta\Omega + \Omega_0^2}, \tag{8}$$

$$b_2 = \frac{4 - 2\Delta\Omega + \Omega_0^2}{4 + 2\Delta\Omega + \Omega_0^2}, \tag{9}$$

where

$$\Delta\Omega = 2\left| \frac{\sin \omega_1 \Delta T}{1 + \cos \omega_1 \Delta T} - \frac{\sin \omega_2 \Delta T}{1 + \cos \omega_2 \Delta T} \right|, \tag{10}$$

$$\Omega_0^2 = \frac{4 \sin \omega_1 \Delta T \sin \omega_2 \Delta T}{(1 + \cos \omega_1 \Delta T)(1 + \cos \omega_2 \Delta T)}. \tag{11}$$

Here ΔT is a sampling interval. Here one assigns the response at certain frequencies ω_0, ω_1 and ω_2. ω_0 is the frequency at which one desires a response of 1.0, ω_1 and ω_2 are two other frequencies around ω_0 where a response of 0.5 is desired. It should be noted that $\omega_0^2 = \omega_1 \omega_2$. To assure a zero phase shift at all frequencies, the filter is first applied in one direction in time and the output is then processed again in the reverse direction in time (Shanks, 1967). The response function of this filter is given by the relation

$$W(Z) = \frac{a(1 - Z^2)}{1 + b_1 Z + b_2 Z^2}, \tag{12}$$

here, $Z = e^{i\omega\Delta T}$. This is called the first-order Butterworth-function filter. The advantage of this method lies in its rapid convergence, freedom in the selection of band widths and its applicability to short data series. Prior to the application of the filter we have detrended the time series of the 365

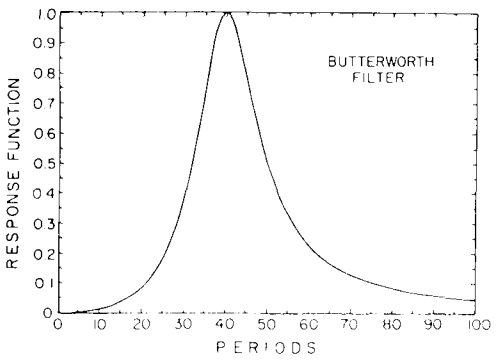

Fig. 2. Response of the band-pass filter plotted as a function of period (days).

days of data by removing the least-square linear trend. Fig. 2 illustrates the response function for the 30 to 50 day filter. Similar, but broader, filters were also used in this study to examine the response in the 24 to 72 day and 30 to 60 day period range.

4.2. Results of the power-spectral calculations

Figs. 3a–h illustrate the raw (unsmoothed) power spectra of the zonal wind at 850 mb for 8 selected points located between 56.25° S and 78.25° N. A more-detailed geographical analysis is presented separately. The abscissa denotes the natural log of the frequency ($l_n \nu$). Considerable power exists at all latitudes in the period range of from 2 to 10 days (ln ν from −0.69 to −2.3).

The amount of variance contained within the period range of 30 to 50 days ($-4 \leqslant \ln \nu \geqslant -3.5$) is also a very conspicuous feature of the power spectra in all of these illustrations. The response over the Asian monsoon region (11.25° N and 67.5° E, as well as 101.25° E) is also very large in this time frame. The equatorial region of the eastern Pacific around 157.5° W also exhibits a very strong response in this period range of 30 to 50 days. Over some of the regions considerable power exists in still lower frequencies. This is particularly true for the monsoon region, where the summer and the winter monsoon responses contain a lot of variance in the annual and the semi-annual components.

It is clearly evident from these illustrations that a broader analysis of the spectra over the globe covering various vertical levels and many variables is necessary to quantitatively describe this phenomenon. The power spectra were accordingly calculated over all of the grid points illustrated in Fig. 1 for 6 vertical levels and 5 variables. A summary of only the major results is presented below, further details will appear in following papers.

4.3. Geographical distributions of power spectra

Since there is no simple representation facilitating the examination of the power spectra over so many grid points, vertical levels, variables and frequencies, illustrations of the % variance distributions for the 30- to 50-day period range will be limited to the following subset (see Fig. 4).

(i) The zonal wind component over the globe at 200 mb (Fig. 4a).
(ii) The zonal wind component over the globe at 850 mb (Fig. 4b).
(iii) The temperature at 300 mb over the globe (Fig. 4c).
(iv) The meridional wind component over the globe at 850 mb (Fig. 4d).
(v) The sea level pressure over the globe (Fig. 4e).

In these illustrations, regions of relatively strong contributions to the % variance in the 30- to 50-day period range have been shaded (see figure captions).

The zonal wind component exhibits large values of % variance along the ITCZ and along the eastern Pacific ocean. This response is evident at the 850 and 200 mb surfaces, especially over the regions of the Asian monsoon. These diagrams of the % variance are somewhat misleading at the higher latitudes. There, the smaller % variances result from the larger variability at the higher frequencies, especially in the 2 to 10 day time frame. However, it is apparent that the relative response in the period range of 30 to 50 days is larger over the tropical belts. The eastern Pacific regions show a meridionally-extending area of larger % variance for the u-component. This is a locality where low-frequency systems have been noted to move meridionally (see section 7).

The contributions to the generation of eddy available potential energy over the tropics is usually large in the upper troposphere, Krishnamurti et al. (1985). Thus, it was felt that a diagram (Fig. 4c) for the % variance of the temperature field at 300 mb might be of interest. Largest variances are noted around 20° S, 15° N and also in the polar latitudes around 70° N and 70° S. A near-equatorial maximum over the central and eastern Pacific ocean may be related to slightly enhanced convection in this region during 1979, which has been identified

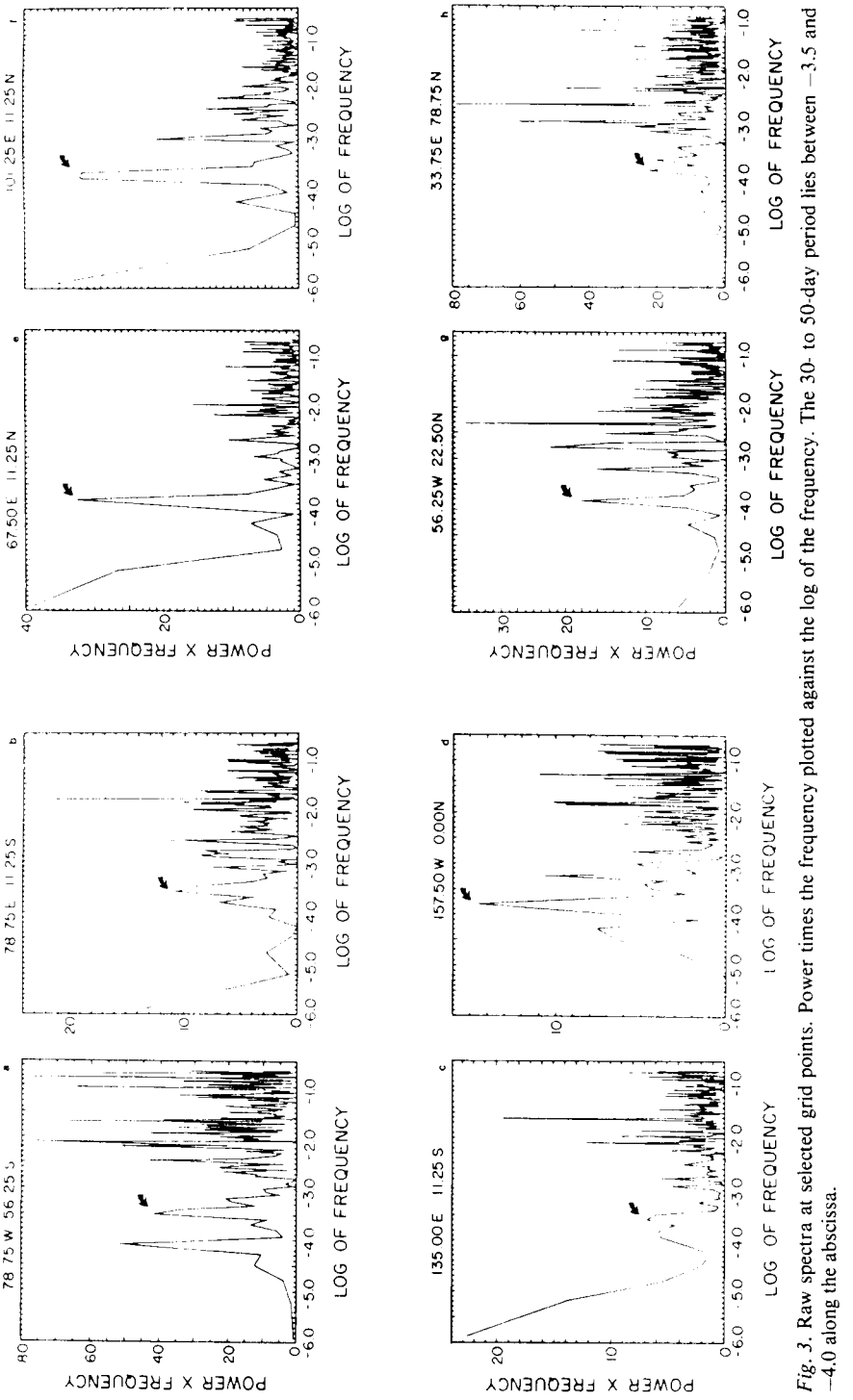

Fig. 3. Raw spectra at selected grid points. Power times the frequency plotted against the log of the frequency. The 30- to 50-day period lies between −3.5 and −4.0 along the abscissa.

as a minor El Niño year. In general, the monsoon and trade wind regions show a larger % variance compared to the equatorial or middle latitudes on this time scale.

The behavior of the specific humidity field at 700 mb usually shows a good response to the fluctuations in the vertical motion field, being low in downward motion areas and high within ascending regions. In general, the % variance appears to be large over the tropical convective areas as well as the subtropical areas where the descending branches of the Hadley and east-west cells (Krishnamurti et al., 1985) are present. Unlike the fields of % variance for the zonal wind and the temperature, the % variance distribution for humidity is uniformly high between roughly 30° N and 30° S compared to the higher latitudes. This strongly suggests that the basic oscillations in the 30 to 50 day time frame may be in the divergent circulations whose upward, as well as the downward, branches respond. As a consequence, this produces a broad response in the humidity field over the entire tropics.

The meridional wind at 850 mb (Fig. 4d) is another variable of considerable interest because of the monsoons and trade wind activity. Aside from these areas, there is also considerable relative variance in the polar latitudes. The final calculation of this sequence is that of the sea level pressure (Fig. 4e). This field, with large relative variances, is quite similar to that for the zonal wind at 850 mb. It appears that the regions of subtropical highs and the monsoon troughs of the summer as well as the winter seasons have large % variances in this period range. This strongly suggests that the divergent circulations over the tropics may also have significant fluctuations on this time scale. This is worthy of exploring, but careful calculation of the vertical motion field from the FGGE data sets is required (Krishnamurti et al., 1985).

4.4. Frequency filtered data at selected locations

A well-known aspect of the frequency filter is that, in the period range of interest, there can be amplitude variation in the different cycles. There are roughly 8 to 12 cycles of the 30 to 50 day oscillations within the 365 days of data. Each cycle does not appear the same; seasonal characteristics are exhibited. Thus, it is of some interest to show the frequency filtered data for selected points around the globe. For this purpose we have selected the same points for which detailed raw spectra were presented earlier (see Fig. 3). The frequency-filtered values of zonal velocity at these same locations are illustrated in Figs. 5a–h. The abscissa in these diagrams denotes days of the FGGE year (from December 1, 1978, through November 30, 1979). Over the southern hemisphere grid points (56.25° S), low-frequency activity is large all year round with amplitude ranges from 2 to 5 m s^{-1}. Over the equatorial Pacific Ocean, (157° W), and the southern Pacific trade wind belt (11° S), the largest activity is found in the southern summer season. Over the southern Indian Ocean trades, the maximum response for the zonal flows occurs somewhat later. Over the Northern Hemisphere (11° N), the largest response is in the summer and fall. During July, the amplitude of the zonal flows at 850 mb approaches 5 m s^{-1}. Over the subtropical (22.5° N) and polar latitudes (78.75° N) the largest low-frequency activity is during the winter season.

A further generalization of this analysis is presented in Section 7, in the form of geographical charts of the low frequency motion field.

5. Vertical structure

The spectra along 90° E and 140° W for the meridional and the zonal wind components are presented in Figs. 6a–d. The spectra are based on 365 days of data at the 1000, 850, 700 500, 300 and 200 mb levels. As stated earlier, wave trains (of the 30 to 50 day mode) propagate meridionally along these two longitudes during the northern summer and the northern winter months, respectively. The meridional and the zonal wind spectra show a peak around 850 mb and 10° N, (Figs. 6c and d). This is largely attributed to the summer monsoon. This region has a pronounced amplitude in the 30- to 50-day period range between the middle of April and early October. It is, however, also of considerable interest here to note that the strongest power in the 30- to 50-day period range is found in the middle and higher latitudes of the upper troposphere. In this context we note that the largest power is found in the upper troposphere around 70° S, 30° S, 30° N and 80° N. At the polar latitudes the phase propagation is generally eastward. Around 30° latitude the

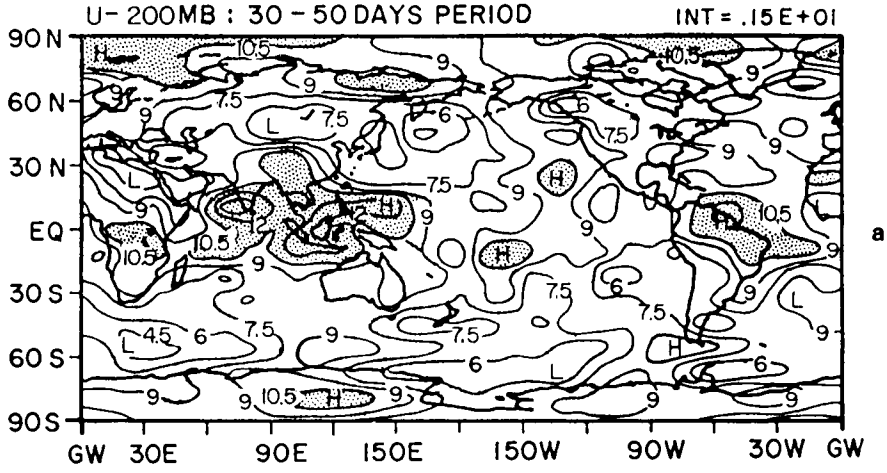
U- 200MB : 30 - 50 DAYS PERIOD
INT = .15E+01
90N
60N
30N
EQ
30S
60S
90S
GW 30E 90E 150E 150W 90W 30W GW

a

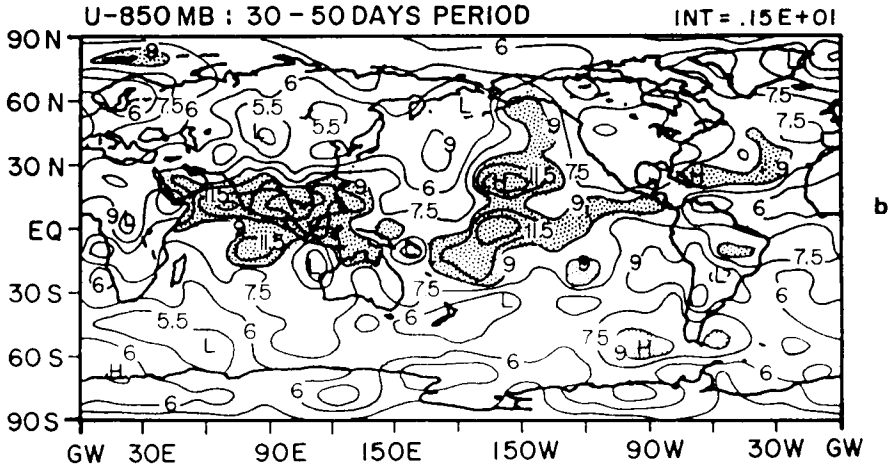
U-850MB : 30 - 50 DAYS PERIOD
INT = .15E+01
90N
60N
30N
EQ
30S
60S
90S
GW 30E 90E 150E 150W 90W 30W GW

b

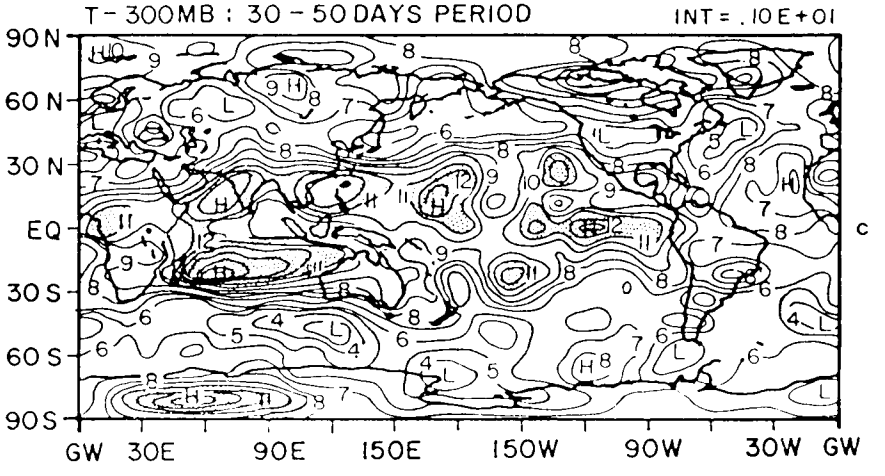
T- 300MB : 30 - 50 DAYS PERIOD
INT = .10E+01
90N
60N
30N
EQ
30S
60S
90S
GW 30E 90E 150E 150W 90W 30W GW

c

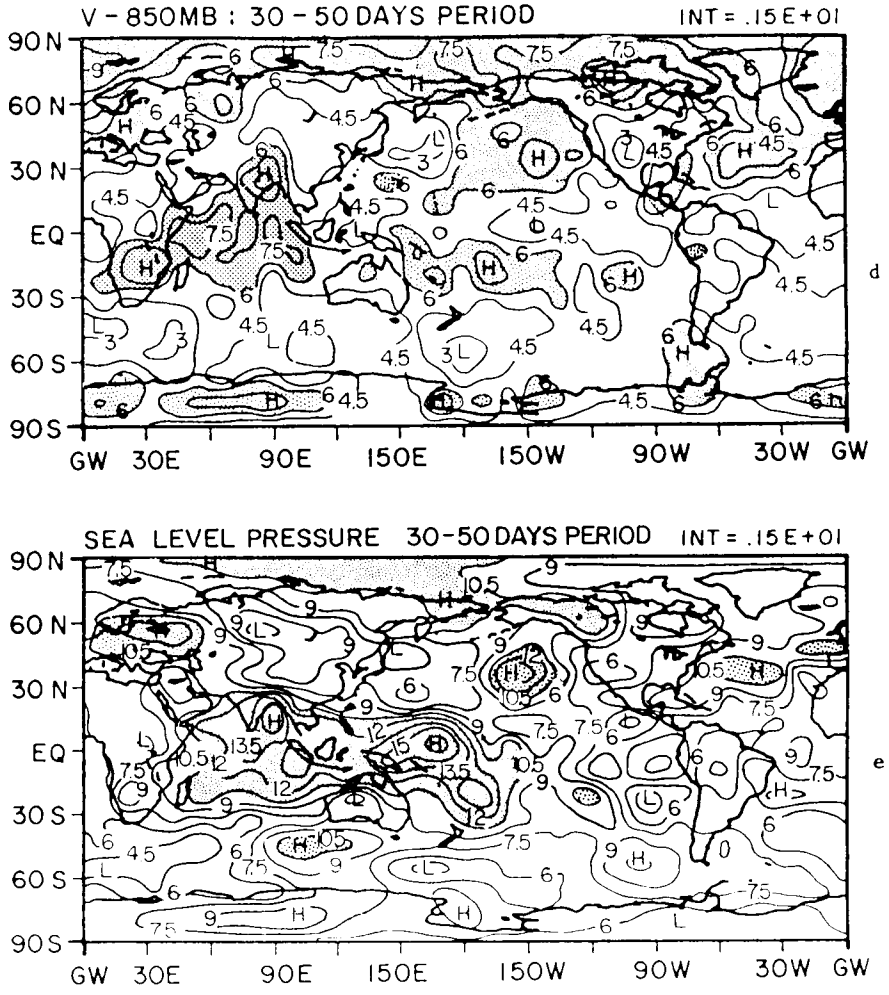

Fig. 4. Geographical distribution of the % variance for the low-frequency (30- to 50-day period range) mode. (a) u component, 200 mb, (b) u component 850 mb, (c) temperature 300 mb, (d) specific humidity 700 mb, (e) meridional velocity v, 850 mb, (f) sea level pressure.

meridional phase propagation is also apparent, especially south of the Himalayas and over the eastern Pacific ocean.

5.1. Barotropic versus baroclinic structure

The essential nature of these disturbances appears to be barotropic, in the sense that the tilt is invariant with altitude (850 and 200 mb). However, we find that the amplitude increases with altitude. Over baroclinic regions where the mean zonal flows increase with height, this nature of barotropic transients (that increasingly draw energy from stronger zonal flow as one proceeds up in the atmosphere) is expected. The directional shear of the low-frequency motions is small, but the amplitude increases somewhat proportional to the mean zonal flow. The ITCZ regions are, however, exceptions to this. Over convective regions of the monsoon between 10° S and 10° N we note a marked non-barotropic character for these low-frequency motions; i.e., the tilt is large and its amplitude is different in the lower and upper troposphere. This aspect was already noted by Krishnamurti and Subrahmanyam (1982). Figs. 6a, b illustrate the vertical structure of the power spectra in the eastern Pacific (140° W). One does

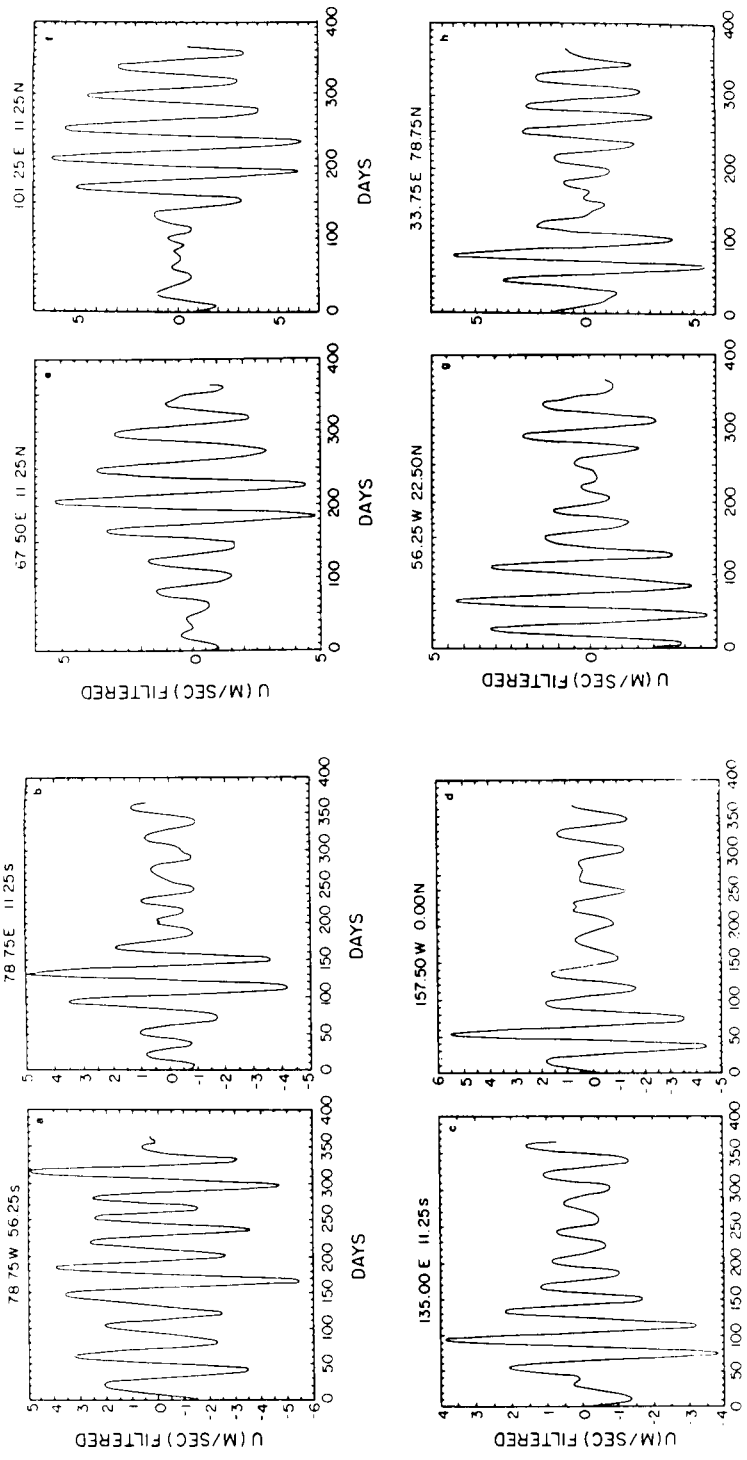

Fig. 5. Frequency filtered data for the zonal velocity at 850 mb (m s^{-1}) for the identical points as in Fig. 3. The abscissa denotes days of FGGE starting from Dec. 1, 1978.

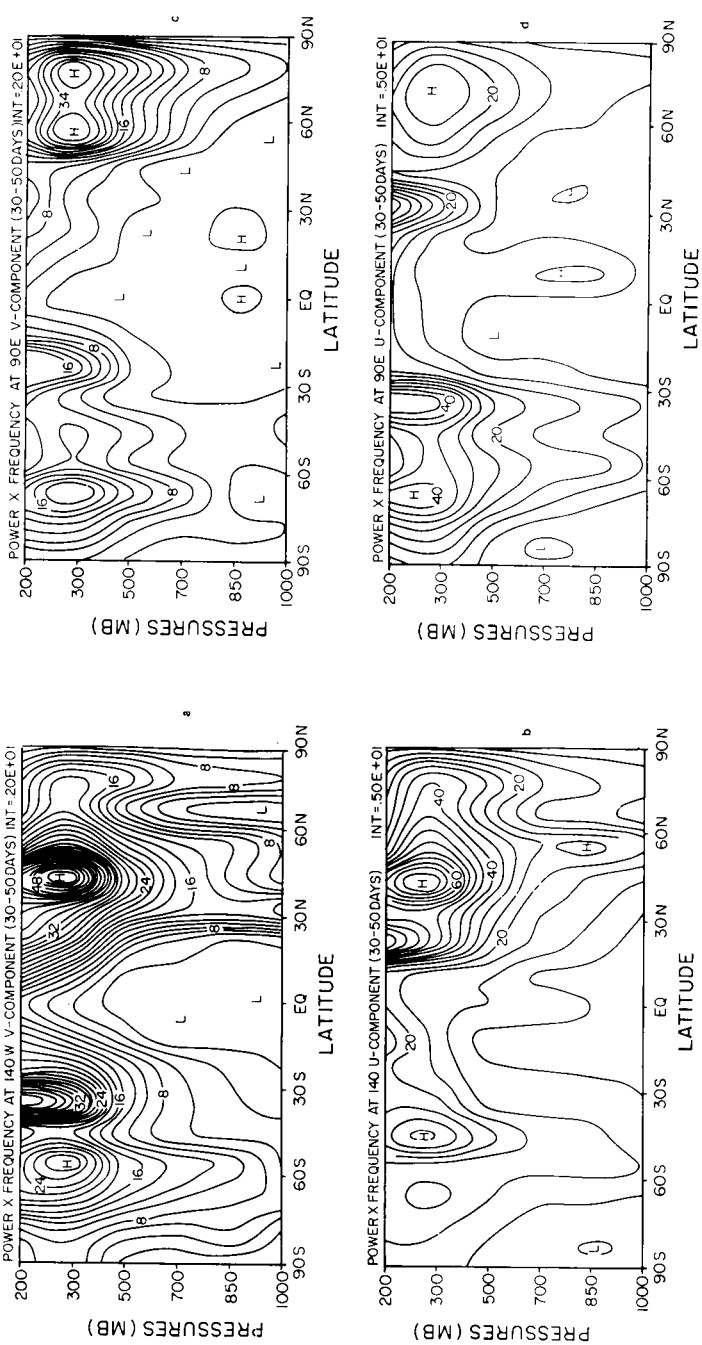

Fig. 6. Vertical distribution of power spectra (power times frequency) analyses as a function of latitude and pressure for the following variables:
(a) v component at 140° W. (b) u component at 140° W.
(c) v component at 90° E. (d) u component at 90° E.
(i) Temperature at 140° W. (j) Temperature at 90° E.
(e), (f), (g), and (h) illustrate the pressure-time section respectively of the zonal wind at selected near equatorial points and at higher latitude points. The location and interval (m s^{-1}) is labelled.

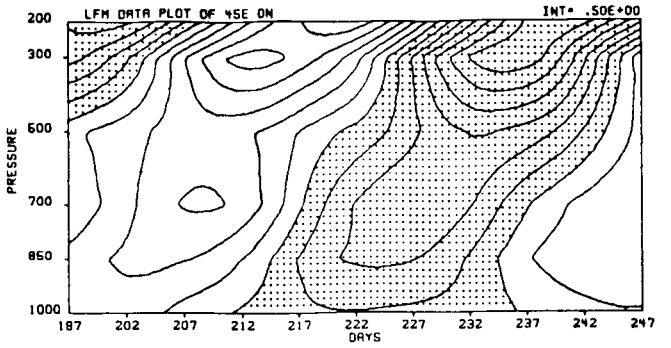

e

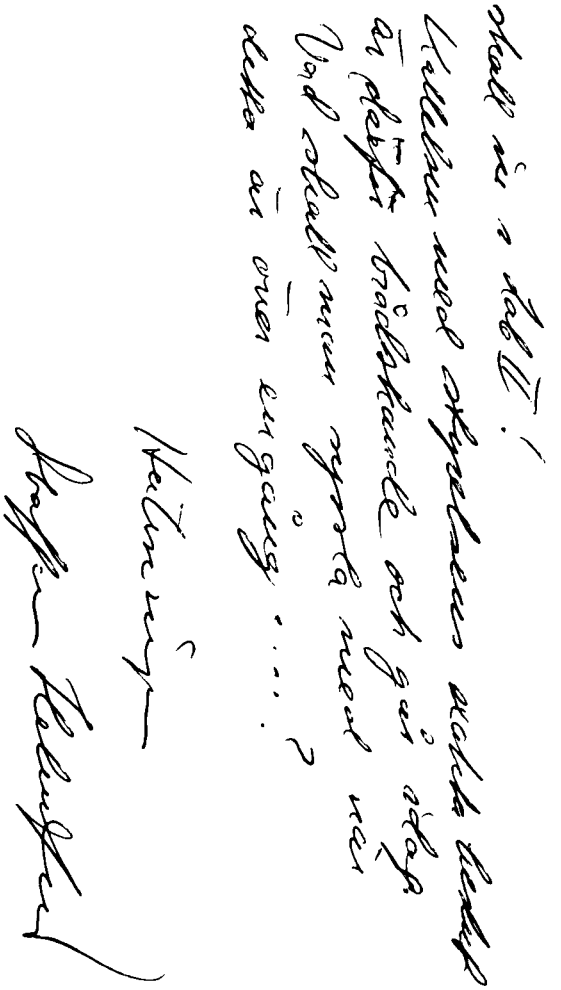

Fig. 6—continued

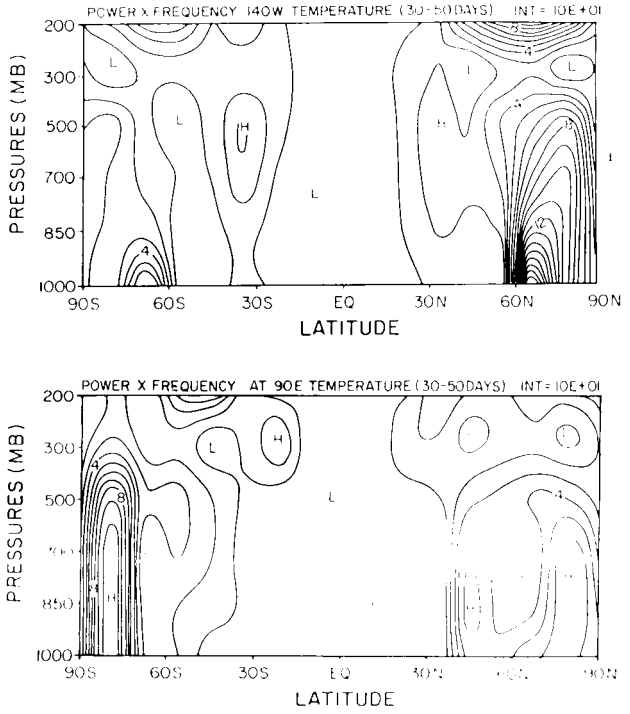

Fig. 6—continued

not find a relative maximum in the power spectral density in the tropical latitudes. At 90° E and 140° W the essential nature of the power spectra for u and v are quite similar—this is because the spectra is largely described by low frequency waves and disturbances. The momentum flux for these low frequency motions has not been investigated. We also noted that the largest power is located on the cyclonic shear side of polar and subtropical jet streams at 90° E and at 140° W. It appears plausible that the horizontal, as well as the vertical shear, may be the sources of energy for the low frequency motions in polar latitudes (Simmons et al., 1983). In this context, diagnostic studies on atmospheric energetics in the frequency domain would be very worthwhile.

5.2. *Phase propagation and excitation source*

The assessment of phase propagation is, usually, very difficult. Traditionally, motion of weather systems are determined from a sequence of weather maps. The Hovmoller type diagrams have been quite useful in determining the eastward (or westward) propagation of wave motions or of different zonal harmonics around latitude circles. Hayashi's (1972) method of analysis of the wavenumber-frequency spectra are extremely useful for delineating the power in the eastward versus westward propagating wave components. There are no simple procedures for assessing phase propagations along the meridional and vertical directions.

The use of a time sequence of low frequency weather maps can provide useful qualitative information on the zonal as well as meridional phase propagation. This approach is followed in Section 7, where a display of such a time sequence of weather maps is presented.

The vertical phase propagation is, here, addressed via a Hovmoller type representation using the vertical-time-sections of the low-frequency zonal winds. The slope of the zero line with increasing time gives a qualitative indication of phase propagation in the vertical plane. Figs.6e–h show four illustrations of these p–t plots of the low frequency zonal winds. The shaded area denotes negative values. The plots in the tropical latitudes exhibit a strong slope suggesting an upward propagation. We show two examples over the tropics (Figs. 6e, f) and two over the extratropical

latitudes (Figs. 6g, h). The tropical examples are presented for the monsoon belt over the Arabian Sea and over the Caribbean during the northern summer. The middle latitude examples are p–t plots over the northern Atlantic and Pacific Oceans. A sharp contrast can be seen in the slope of the systems over the tropics and middle latitudes.

In general, we note a strong coherence of phase among adjacent vertical levels. The entire p–t plots as well as their horizontal structure appears to be highly ordered. The time series analysis and the frequency filtering is carried out quite independently at each x, y, p location and the frequency filtered data are cast back into these different representations. The space-time continuity of phase suggests that a well-defined low-frequency oscillation indeed exists over most of the troposphere. The slope of the low frequency systems over the tropics in general show an upward phase speed of roughly 800 mb per 20 days. In the extratropical latitudes the lack of vertical slope suggests a more barotropic character for the 30 to 50 day oscillations.

We shall next illustrate the meridional/vertical structure of the power spectra at 140° W and 90° E for the temperature field (Fig. 6i,j). The variance of the temperature field Figs. 6i,j) shows the largest power in the polar latitudes, where the low-frequency motion field has also its largest amplitude. The tropical temperature field has very little response in this period range at 90° E and 140° W; this is true of most of the tropics. It is not clearly apparent why the power of the temperature field is largest around 70° S and 70° N in the lower troposphere in this frequency range.

5.3. *Low-frequency system cross sections*

It is of interest to examine vertical cross sections across individual troughs and ridges of the low frequency systems. The quasi-barotropic nature of the low-frequency systems away from convective regions is well brought out by such cross sections. We shall present these for two individual days (July 2, 1979 and December 31, 1978) in order to illustrate structure along 90° E and 140° W. The parameters shown here are the vertical component of the relative vorticity (Fig. 7a), and the zonal wind (Fig. 7b). Although there is an increase of amplitude with height in the convective areas

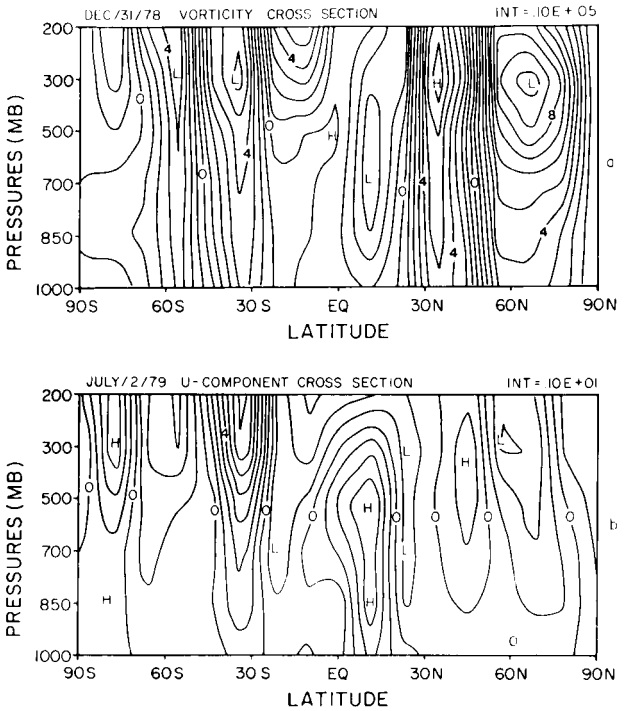

Fig. 7. Vertical cross sections of frequency-filtered fields. (a) Absolute vorticity along 140° W. Interval = 0.1 × 10^{-5} s^{-1}. (b) Zonal velocity along 90° E. Interval 1 m s^{-1}.

(10° N for July and 5° N for December), in general the isopleths are vertically oriented over most of the cross section, affirming the essentially barotropic character of these low frequency motions. We have intercompared cross sections and the time sections at numerous longitudes and individual grid points, the phenomenon appears to have a large scale structure in space along x, y and p.

6. Some seasonal aspects at 850 mb

Using the filtered zonal and meridional wind component data set for the entire year at each grid point, it is possible to illustrate maximum wind charts for each of the four seasons. Reference should be made to graphs shown in Fig. 5 for the definition of maximum wind used here. In this data set, which is 365 days long, roughly 7 to 10 oscillations of the zonal wind occurs. We have selected "the maximum zonal wind" from these oscillations to depict these charts for each season separately. Here the seasons are defined as follows:

winter: December 1, 1978, through February 28, 1979;
spring: March 1, 1979, through May 31, 1979;
summer: June 1, 1979, through August 31, 1979;
autumn: September 1, 1979, through Nov. 30, 1979.

Figs. 8a–d illustrate the amplitude of the maximum wind for each of the four seasons. The largest amplitude of the maximum wind generally occurs in the middle latitudes where magnitudes as large as 6 to 8 m s^{-1} are attained.

6.1. *Winter*

During the winter of 1978–79, the largest amplitudes are found over the northern Atlantic and Pacific Oceans. This clearly shows that the Aleutian and Icelandic lows exhibit a strong low-frequency component on the time scale of 30 to 50 days. Another region of strong winds is located over the Caspian Sea where the maximum wind reaches magnitudes close to 6 m s^{-1}. The winter monsoon region over East Asia, South China Sea, Borneo, Malaysia, Indonesia and northern Australia does not exhibit large amplitudes on this time scale. This region has been investigated in considerable detail by Quah (1983) who has noted this same behavior. The equatorial regional near 160° W shows maximum winds around 5.5 m s^{-1} during the northern winter season. In Section 7, we will identify this as a source region for the low frequency systems. The southern hemisphere shows maximum winds around 60 to 70° S. On the whole, the most active belt is located near 55° N during this period.

6.2. *Spring*

The northern spring months show (Fig. 8b) an enhancement of amplitudes in the southeastern Pacific ocean around 90° W, where winds attain a magnitude of 7 m s^{-1}. During these months a monsoonal wind maxima appears over southern Indochina and Malaysia. The strongest amplitude of the low-frequency wind maxima is found over the northern Atlantic ocean near 50° N with amplitudes around 8 m s^{-1}. These strong winds are associated with slow eastward-moving, large scale disturbances that interact with higher frequency motions such as frontal cyclones, with corresponding enhancement in the local circulations and associated weather activity. This is illustrated in Section 7.

6.3. *Summer*

During the northern summer months (Fig. 8c), we note the strongest zonal winds over the region of the Asian summer monsoons. This was noted by Krishnamurti and Subrahmanyam (1982) from an earlier analysis of the summer monsoon data sets. The present study utilizes a more robust time series of 365 days of wind data and confirms this finding. The axis of strong wind activity extends from the Arabian Sea around 10° N to roughly 20° N over the western Pacific Ocean. The southern Pacific Ocean shows considerable low-frequency activity, with maximum winds exceeding 4 m s^{-1} cover a large part of this ocean. The maximum amplitude during northern summer is found near 60° to 70° S where magnitudes as large as 6 m s^{-1} are noted.

6.4. *Autumn*

During the northern autumn months (Fig. 8d), the amplitude of low-frequency maximum winds diminishes over the region of the Asian monsoons. The largest amplitude of low-frequency activity is found along 50° S, especially in the southern Pacific and southern Indian Oceans where amplitudes exceed 5 m s^{-1}. In this region, low-

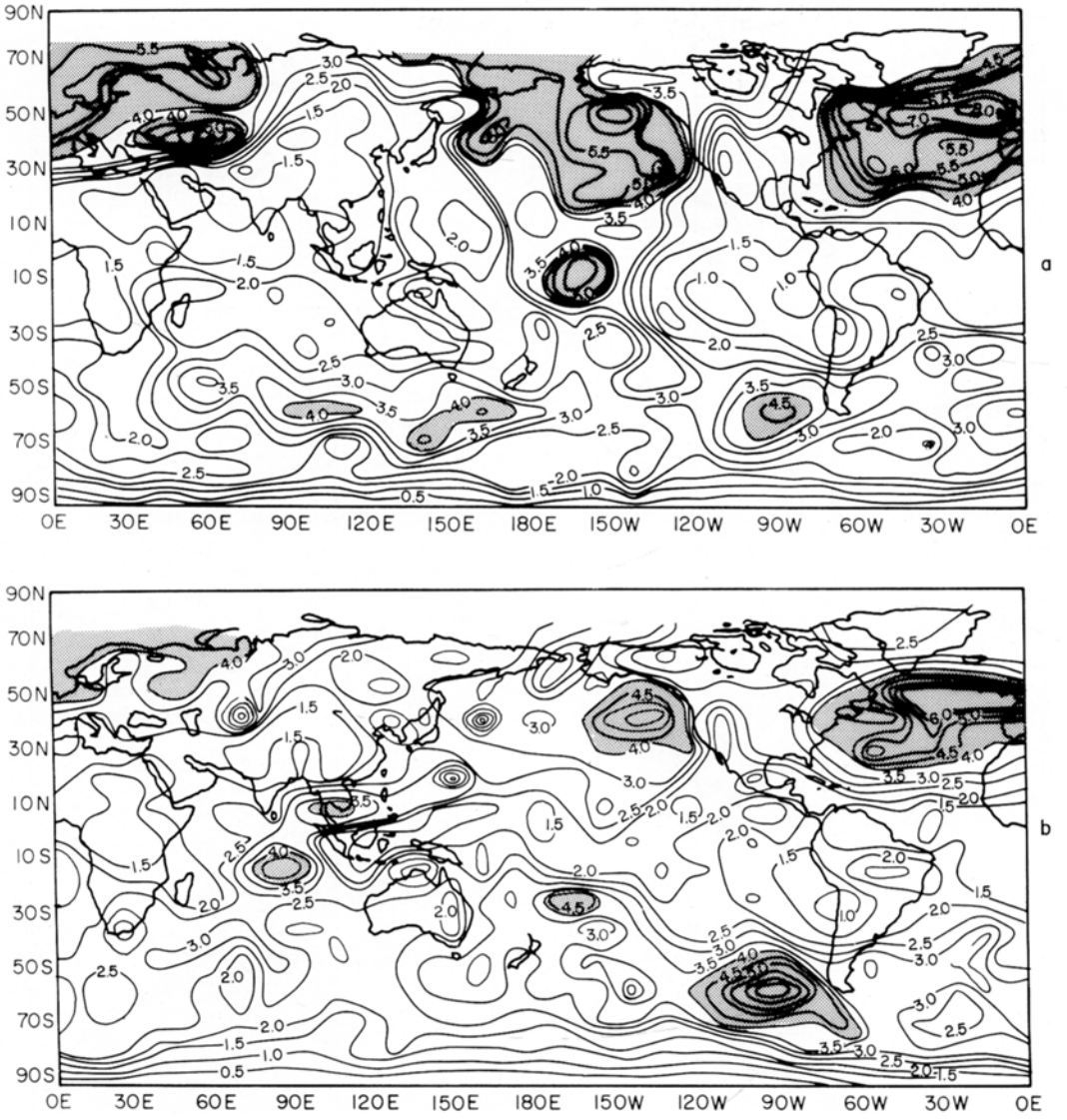

Fig. 8. Maximum zonal wind at 850 mb of frequency-filtered motions during individual seasons (m s^{-1}). (a) Winter. (b) Spring. (c) Summer. (d) Autumn.

frequency disturbances generally move eastward. As stated earlier, the maximum amplitude of the low frequency motions generally occur in the middle latitudes poleward of 45°.

7. Low-frequency 'storms'

When the entire FGGE year of data is time filtered and the motion fields extracted, three features become quite evident.

(i) Well-defined (cyclonic and anti-cyclonic) features are very coherent on large spatial scales.

(ii) Many 'storms' (cyclonic or anti-cyclonic) are stationary, but some are noted to move meridionally. The rate of propagation of these systems is roughly 1° latitude per day. In the higher latitudes, especially near the belt of strong westerlies of the annual mean flow (around 60° S and 60° N), these anomalies tend to move generally eastwards.

(iii) A number of low-frequency "storms" are

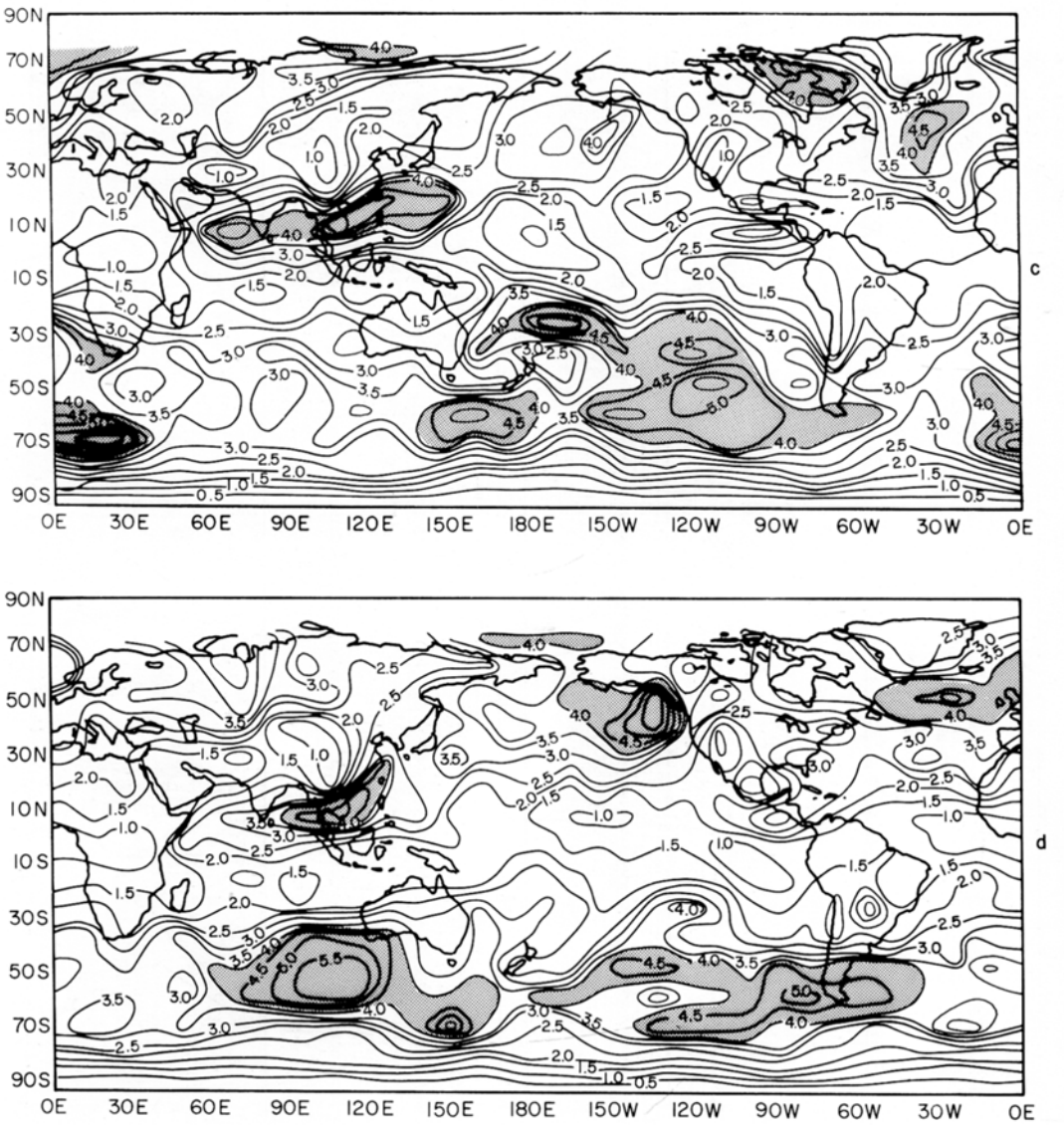

Fig. 8—continued

long lasting and exist longer than the 30 to 50 day time scale. In this context, it is worth emphasizing again that, other than the initial analysis of the FGGE IIIb charts, one does not build in any spatial inter-relationship in the filtered data sets between the different grid points. All points are independently time filtered and subsequently recombined as weather maps. Thus, the long-lasting moving "storm" indicates a time evolution of phase of a large amplitude, low-frequency event.

In this context, one always has some reservations about the sensitivity of the results to the width of a time filter. Our interest in this study is on events close to the 40 day period. In this context we examined low-frequency charts for three different period ranges:

(i) 30 to 50 days which is illustrated here;
(ii) 24 to 72 days;
(iii) 30 to 60 days.

There were almost no major differences in the

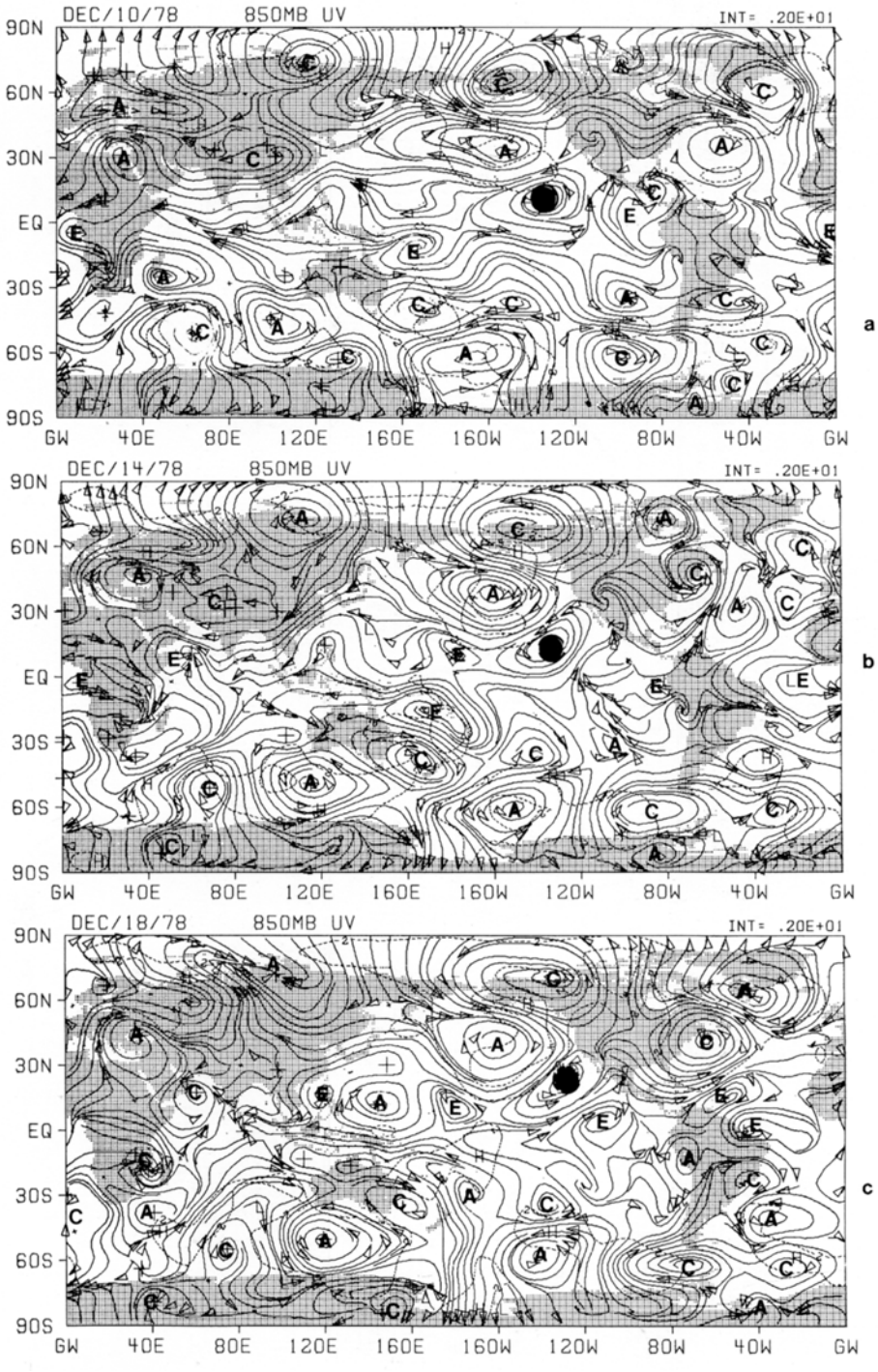

Fig. 9. Frequency-filtered streamline charts at 850 mb at 4-day intervals starting from December 10, 1978. The heavy black dot denotes a long lasting low-frequency storm.

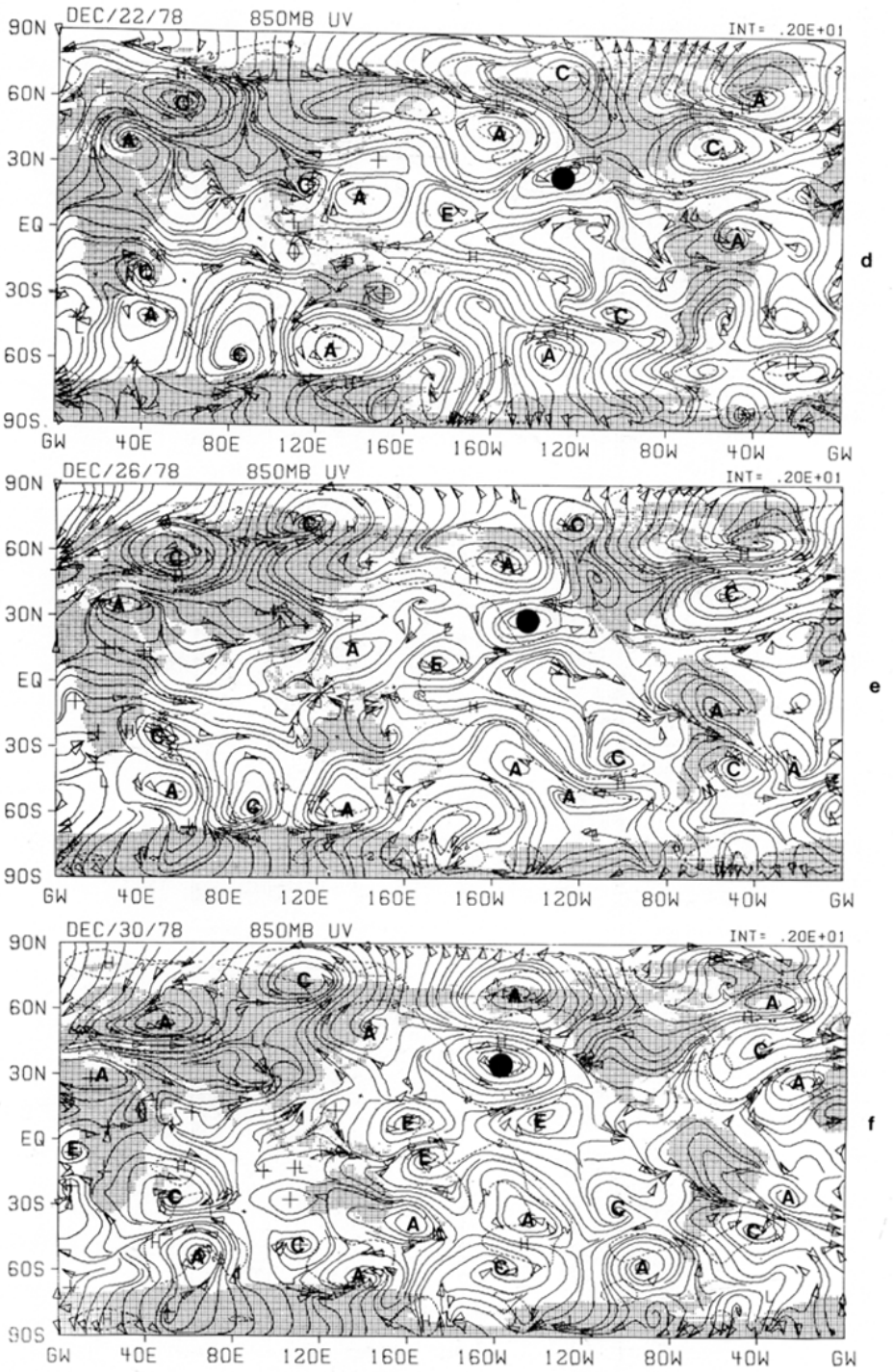

Fig. 9—continued

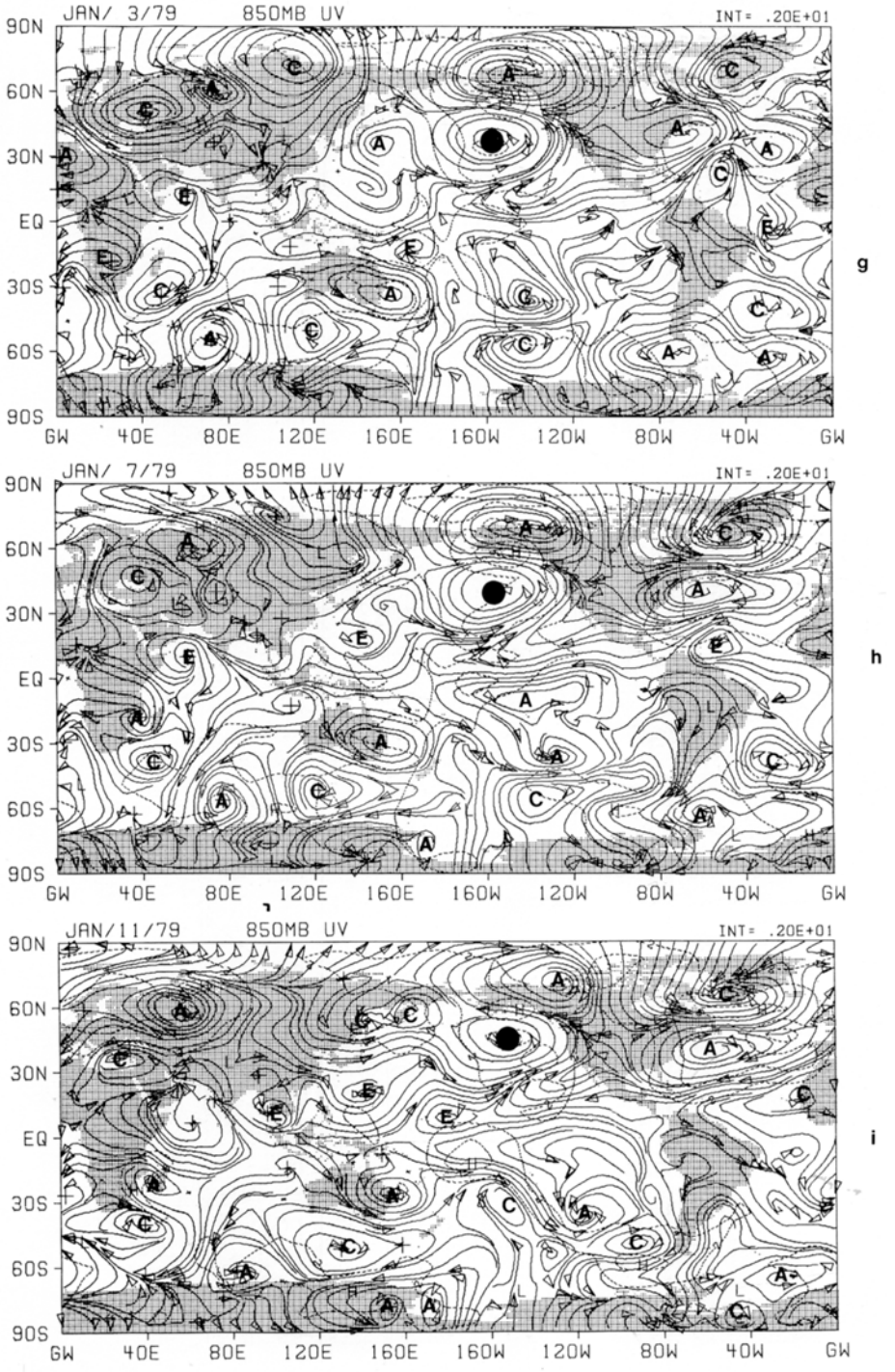

Fig. 9—continued

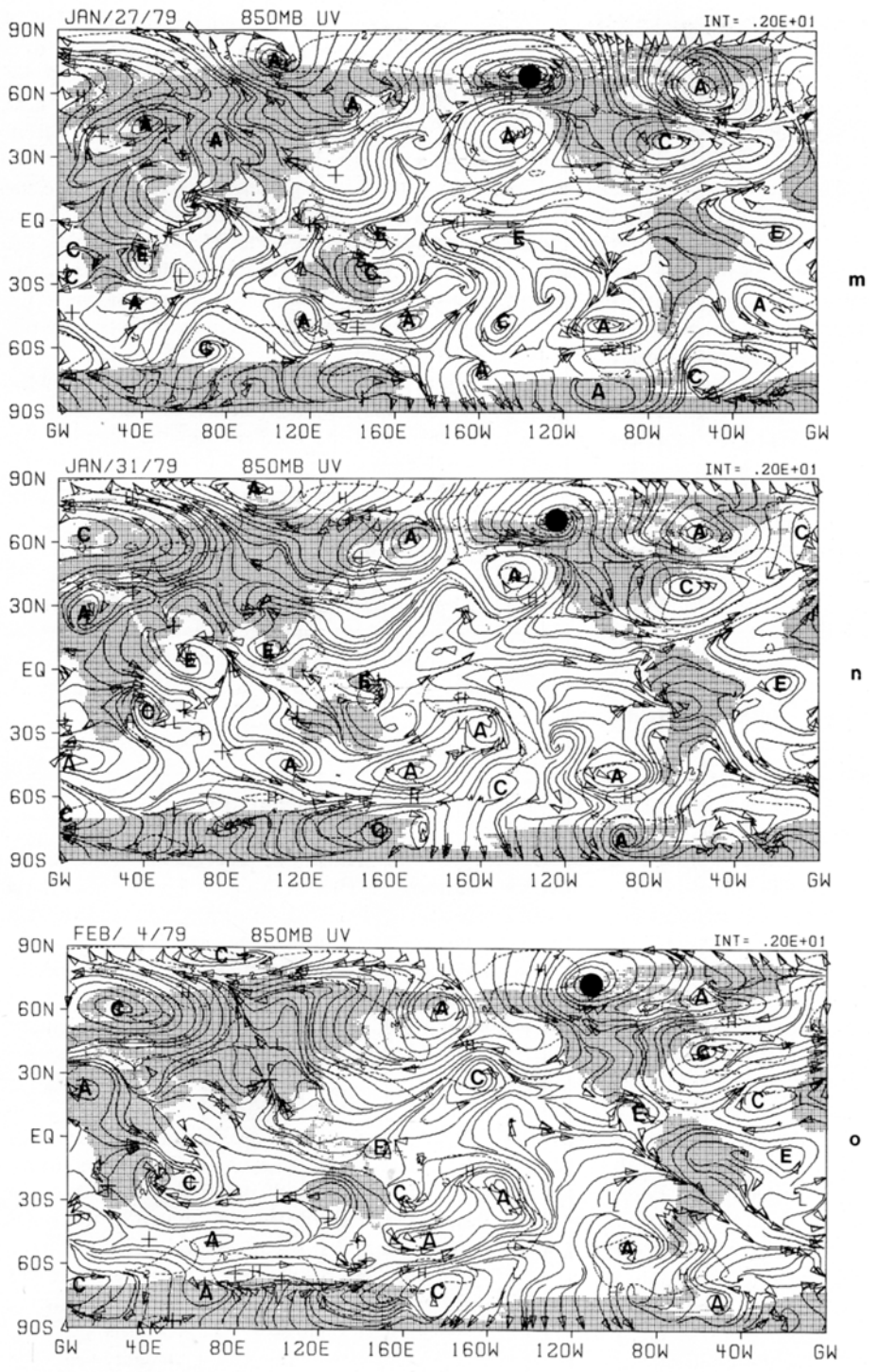

Fig. 9—continued

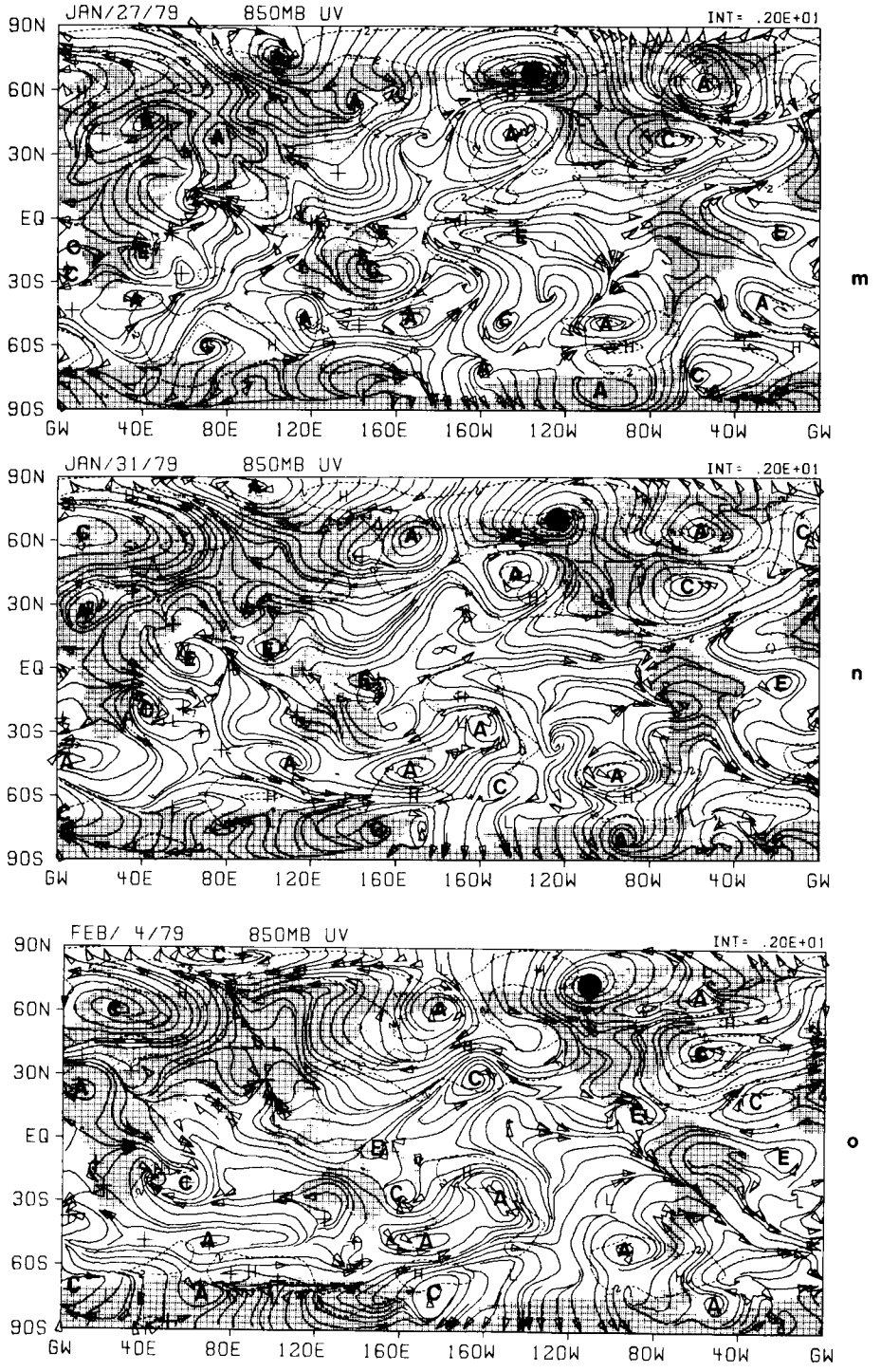

Fig. 9—continued

features. Such a calculation was necessary to examine if the results might not be a function of the narrowness of the filter. "Storm" for "storm" one can identify the same elements in the three different band-pass representations. Here we shall present two sequences of charts from the 30 to 50 day filtered field to illustrate low-frequency "storms". The streamlines and isotachs at 850 mb for the period December 10 through February 28, 1979 at intervals of 4 days are shown in Figs. 9a through u. Here the cyclonic and anti-cyclonic disturbances are indicated by the letters C and A, respectively. The near-equatorial disturbances are identified by the usual letter E to signify eddies whose cyclonic or anti-cyclonic character is not definable. Among these we have blackened out the center of a propagating long lasting low-frequency "storm". Although many of the centers shown in Fig. 9 exhibit interesting evolution of phase it is impossible to discuss each of these in this preliminary study. We shall concentrate on two of these that appear most striking during the Northern winter and summer seasons.

8. The December 1978 case study

In the December sequence of charts, such a long-lasting anomaly is first noted on December 10, 1978 around roughly 140° W and 10° N. This "storm" slowly moves northwards. It approaches 25° N by December 18th and 30° N by December 30th. By January 11th this perturbation is located around 45° N and 140° W. By January 23rd it approaches the Alaskan region near 60° N and has winds around it of the order of 6 m s^{-1}. Hereafter, the "storm" commences a rapid eastward motion approaching around 100° W and 70° N by February 4. By February 16th its position can be seen around 50° W and 60° N. In the final chart, shown for February 28, this low frequency "storm" approaches 20° W and 60° N. Although the maps are not shown for the latter period, this "storm" was noted to continue an eastward motion until around March 20 when, barely discernible, it was located over Siberia near 60° E as it lost its amplitude and disappeared. This "storm" had a life span of around 80 days. This type of "storm" is of particular importance for various obvious reasons. When this "storm" was in subtropical latitudes the maximum winds around the "storm" were around 2 m s^{-1}, however, as it approached the Gulf of Alaska its winds reached an amplitude of over 6 m s^{-1}. A low-frequency "storm" of this size (5000 km from adjacent ridge to ridge) stays near the Gulf of Alaska for a fairly long time. Meanwhile a number of high-frequency "storms" go by this region. The high-frequency "storms" are the polar front cyclones and anti-cyclones that move eastward at a rate of about 15° longitude/day. The general cyclonic circulation is thus considerably enhanced during periods of superposition of the high and low-frequency "storm" events over this general region.

In addition, we have also examined in detail the low-frequency motion field over the monsoon region during the northern summer months. The FGGE data confirms the northward passage of a family of troughs and ridges from the equatorial region towards the Himalayas. The passage of these troughs and ridges, in the 850 mb motion field, appears to be closely related to the wet and dry spells of weather over central India. Further details of these low-frequency motions over the monsoon region are described in Krishnamurti and Subrahmanyam (1982) and Krishnamurti et al. (1985).

9. Concluding remarks

The 30- to 50-day oscillations have drawn considerable interest in recent years. Sea level pressure and related divergent motions exhibit a large variance on this time scale in the equatorial latitudes. These are largely described by planetary scale eastward propagating waves. The present study confirms the importance of those oscillations over the tropics as well as over higher latitudes.

9.1. Power-spectral analyses

The power-spectral analysis of the year-long data sets of FGGE shows a strong response in the period range of 30 to 50 days over the region of the Asian monsoons, the tropical convective zones and the polar latitudes. A marked response exists in the spectra of the zonal winds of the tropical lower and upper troposphere and the polar latitudes. A strong response is also noted in the sea level pressure, temperature at 300 mb and the humidity field. The distribution of the frequency-filtered fields strongly suggests that the 30- to 50-day oscillations are

closely linked to tropical convection and associated divergent circulations. The broad response of the humidity field over most of the tropics suggests that the ascending as well as the descending branches of the divergent circulations (that encompass most of the tropics) undergo these oscillations.

9.2. Band-pass filtered analyses

Frequency-filtered fields show responses in the zonal winds that are as large as 8 m s^{-1} over polar latitudes. The day-by-day display of these fields suggests interactions among the low- and high-frequency events of the higher latitudes. Some major developments of the Aleutian and Icelandic lows during FGGE were traced to the superposition of low-frequency perturbations and the passage of higher-frequency cyclones. The low-frequency "storms" appear as well-defined entities on these charts. While most regions seem to experience standing oscillations on this period range, meridionally-propagating trough/ridge systems and closed circulations were also found over the region of the Asian summer monsoon and over the eastern Pacific Ocean. Zonally-propagating, low-frequency storms were found over the polar latitudes near 60° N. The scale of these storms is on the order of 4000 km; they seem to preserve a steady propagation of phase for long periods and seem to have a lifetime larger than the period range of 30 to 50 days. Away from convective regions, low-frequency disturbances appear to be barotropic. Over the convective regions an upward phase propagation was evident in our analyses.

9.3. Excitation sources

In this study, we have presented interesting time-pressure diagrams of the zonal velocity on this time scale at different locations. A strong upward tilt with time over tropical latitudes and a lack of it over the extratropical latitudes suggests that the energy source for these oscillations may be in low latitudes.

One possibility for the source of excitation of these low-frequency events is a self oscillation of tropical convection due to surface energy input as postulated by Krishnamurti and Bhalme (1976) and Webster (1983). Other possibilities include symmetric instability of the shear flows in low latitudes (Anderson and Rosen, 1983; Stevens, 1983; Dunkerton, 1983).

The much larger amplitude of the low-frequency motions in the period range of 30 to 50 days at the polar latitudes also raises another possibility for this scenario: it is conceivable that a low-frequency component of baroclinic instability exists over the high latitudes. This may lead to giant "storms" in the middle latitudes that, in turn, exert a marked influence on low-latitude events, i.e., the eddy heat and momentum-flux forcing. The tropical events, including an enhancement of the tropical convection, attendant divergent circulations and pressure oscillations, and associated zonal wind oscillations could all be thus viewed as a response to the higher latitude forcing.

The observational aspects of this phenomenon needs to be reexamined with several more years of observations. The ultimate understanding of the mechanisms responsible for the excitation of motions on this time scale will undoubtedly come from modelling efforts. At this stage it is not apparent that current general circulation models have successfully simulated some of these gross observational features.

10. Acknowledgements

Dr. M. Murakami and Phillip Ardanuy provided assistance in clarifying many aspects of this study. We wish to express our gratitude to the European Center for Medium Range Weather Forecast Group for the excellent FGGE IIIb data sets. This research was supported by the National Science Foundation (NSF), grant number ATM 78-19363. The calculations reported here were carried out at the computer facility of the National Center for Atmospheric Research (NCAR) which is sponsored by the National Science Foundation.

REFERENCES

Anderson, J. R. and Rosen, R. D. 1983. The latitude-height structure of 40–50 day variations in atmospheric angular momentum. *J. Atmos. Sci. 40*, 1584–1591.

Bengtsson, L., Kanamitsu, M., Kållberg, P. and Uppals, S. 1982. FGGE 4-dimensional data assimilation at ECMWF. *Bull. Amer. Meteorol. Soc. 63*, 29–43.

Chang, Chih-Pei 1977. Viscous internal gravity waves and low-frequency oscillations in the tropics. *J. Atmos. Sci. 34*, 901–910.

Dunkerton, T. J. 1983. A nonsymmetric equatorial inertial instability. *J. Atmos. Sci. 40*, 807–813.

Endlich, R. M., Singleton, R. C. and Kaufman, J. W. 1969. Analysis of detailed vertical wind speed profiles. *J. Atmos. Sci. 26*, 1030–1041.

Guillemin, E. A. 1957. *Synthesis of passive networks.* Wiley, 571 pp.

Hayashi, Y. 1972. A method of analyzing transient waves by space-time cross spectra. *J. Appl. Meteorol. 12*, 404–408.

Krishnamurti, T. N. and Bhalme, H. N. 1976. Oscillations of a monsoon system. Part I: Observational aspects. *J. Atmos. Sci. 33*, 1937–1953.

Krishnamurti, T. N. and Subrahmanyam, D. 1982. The 30–50 day mode at 850 mb during MONEX. *J. Atmos. Sci. 39*, 2088–2095.

Krishnamurti, T. N., Jayakumar, P. K., Sheng, J., Surgi, N. and Kumar, A. 1985. Divergent circulations on the 30- to 50-day time scale. *J. Atmos. Sci. 00*, 000–000.

Lorenc, C. 1980. A global three-dimensional multivariate statistical interpolation scheme. *Mon. Wea. Rev. 109*, 701–721.

Lorenc, C. 1984. The evolution of planetary scale 200 mb divergences during the FGGE year. Meteorological office Technical note No. II/210, pp. 1–23. Available from Dynamical Climatology Branch, Meteorological Office, London Road, Bracknell, Berkshire, England.

Madden, R. A. and Julian, P. R. 1971. Detection of a 40–50 day oscillation in the zonal wind in the tropical Pacific. *J. Atmos. Sci. 28*, 702–708.

Madden, R. A. and Julian, P. R. 1972. Description of global-scale circulations cells in the tropics with a 40–50 day period. *J. Atmos. Sci. 29*, 1109–1123.

Murakami, M. 1979. Large-scale aspects of deep convective activity over the GATE area. *Mon. Wea. Rev. 107*, 994–1013.

Murakami, M. 1983. Analysis of the deep convective activity over the western Pacific and southeast Asia. Part I: Diurnal variation. *J. Meteorol. Soc. Japan 61*, 60–76.

Murakami, M. 1984. Analysis of deep convective activity over the western Pacific and Southeast Asia. Part II. *J. Meteorol. Soc. Japan 62*, 88–108.

Murakami, T., Nakazawa, T. and Jin Hai He 1983. 40–50 day oscillations during the 1979 Northern Hemisphere summer. Technical Report No. UHMET 83-02. Department of Meteorology, University of Hawaii, Honolulu, Hawaii.

Quah, Leong-Chuan 1983. On the 30–50 day tropospheric oscillation during the 1978–79 Northern Winter. Masters Thesis, Department of Meteorology, Florida State University, Tallahassee, Florida, 32306.

Shanks, J. C 1967. Recursion filters for digital processing. *Geophysica 32*, 33–51.

Sikka, D. R. and Gadgil, S. 1980. On the maximum cloud zone and the ITCZ over Indian Longitudes during the southwest monsoon. *Mon. Wea. Rev. 108*, 1840–1853.

Simmons, A. J., Wallace, J. M., Branslator, G. W. 1983. Barotropic wave instability and atmospheric teleconnection patterns. *J. Atmos. Sci. 40*, 1363–1392.

Stevens, D. E. 1983. On symmetric stability and instability of zonal mean flows near the equator. *J. Atmos. Sci. 40*, 882–908.

Webster, P. J. 1983. Mechanisms of monsoon low-frequency variability: surface hydrological effects. *J. Atmos. Sci. 40*, 2110–2124.

Yasunari, T. 1981. Structure of an Indian summer monsoon system with around 40-day period. *J. Meteorol. Soc. Japan 59*, 336–354.

Yasunari, T. 1980. A quasi-stationary appearance of 30- to 40-day period in the cloudiness fluctuations during the summer monsoon over India. *J. Meteorol. Soc. Japan 58*, 225–229.

Zangvil, A. 1977. On the presentation and interpretation of spectra of large-scale disturbances. *Mon. Wea. Rev. 105*, 1469–1472.